Ingeniería y Ciencia, ISSN 1794–9165
Volumen 4, número 8, diciembre de 2008, páginas 99–128

Numerical treatment of cosserat based rate independent strain gradient plasticity theories

Tratamiento numérico de una teoría de plasticidad por gradiente de deformación basada en un modelo de cosserat

Juan David Gómez C.[1]

Recepción: 23-abr-2008/Modificación: 16-oct-2008/Aceptación: 16-oct-2008
Se aceptan comentarios y/o discusiones al artículo

Abstract
The current trend towards miniaturization in the microelectronics industry has pushed for the development of theories intended to explain the behavior of materials at small scales. In the particular case of metals, a class of available non–classical continuum mechanics theories has been recently employed in order to explain the wide range of observed behavior at the micron scale. The practical use of the proposed theories remains limited due to issues in its numerical implementation. First, in displacement–based finite element formulations the need appears for higher orders of continuity in the interpolation shape functions in order to maintain the convergence rate upon mesh refinement. This limitation places strong restrictions in the geometries of the available elements. Second, the available inelastic constitutive models for small scale applications have been cast into deformation theory formulations limiting the set of problems to those exhibiting proportional loading only. In this article two contributions are made for the particular case of a Cosserat couple stress continuum. First it describes a numerical scheme based on a penalty function/reduced integration approach that allows for the proper treatment of the higher order terms present in Cosserat like theories. This scheme results in

[1] PhD in computational mechanics, jgomezc1@eafit.edu.co, associate professor, applied mechanics group, EAFIT University, Medellín–Colombia.

a new finite element that can be directly implemented into commercial finite element codes. Second, a flow theory of plasticity incorporating size effects is proposed for the case of rate independent materials overcoming the limitations in the deformation theory formulations. The constitutive model and its corresponding time–integration algorithm are coupled to the new proposed finite element and implemented in the form of a user element subroutine into the commercial code ABAQUS. The validity of the approach is shown via numerical simulations of the microbending experiment on thin Nickel foils reported in the literature.

Key words: non–classical continuum theories, Cosserat continuum medium theory, couple stress theory, small scale inelastic response, finite element analysis, constitutive modeling, integration algorithms.

Resumen

La tendencia actual hacia la miniaturización en la industria microelectrónica ha promulgado el desarrollo de teorías orientadas a explicar el comportamiento de materiales usados en pequeña escala. En el caso particular de los metales, recientemente se ha usado una clase de teorías no clásicas de la mecánica de los medios continuos con el fin de explicar una amplia gama de observaciones a escala micrométrica. Sin embargo el uso práctico de las teorías propuestas permanece limitado debido a dificultades a la hora de su implementación numérica. En primer lugar, cuando éstas van a ser implementadas en formulaciones por elementos finitos basadas en desplazamientos se genera la necesidad de altos órdenes de continuidad en las funciones de interpolación con el fin de mantener las propiedades de convergencia en el algoritmo. Estas limitaciones generan fuertes restricciones en las geometrías de los elementos disponibles. De otro lado, los modelos inelásticos disponibles para aplicaciones a pequeña escala han sido formulados como teorías de deformación (total) limitando su aplicabilidad a problemas bajo condiciones proporcionales de carga. En el presente artículo se hacen dos contribuciones para el caso de un continuo de Cosserat con tensiones de par. Primero se describe un esquema numérico basado en una estrategia de funciones de penalización combinadas con integración reducida para abordar apropiadamente el problema de los términos de orden superior presentes en la teoría de los Cosserat. Este esquema da como resultado un nuevo elemento finito que puede ser directamente acoplado a programas de distribución comercial que acepten subrutinas de usuario. En segundo lugar se propone una teoría de flujo de plasticidad incorporando efectos de tamaño superando algunos de los obstáculos de las teorías por deformación. El modelo constitutivo resultante y su correspondiente esquema de integración en el tiempo son acoplados al nuevo elemento formulado e implementados en subrutinas de usuario de ABAQUS. La validez de la estrategia es demostrada mediante simulaciones del ensayo de microflexión en láminas de níquel reportados en la literatura.

Palabras claves: teorías no clásicas del continuo, teoría del continuo de Cosserat, teoría de tensiones de par, respuesta inelástica a pequeña escala, análisis por elementos finitos, modelación constitutiva, algoritmo de integración.

1 Introduction

1.1 The size effects problem associated to non-uniform inelastic fields

Recent developments in the microelectronics industry and other related problems (like the emerging nanotechnology) have pushed for a strong interest in continuum mechanics theories applicable at the small scale level, (micron or even sub-micron scale). Of particular interest is the so-called size effects problem that has been experimentally observed in many metals and its alloys and where a resistance parameter seems to increase in the direction of decreasing specimen size. Under elastic conditions this behavior appears to be important only when the specimen size becomes comparable to typical inter-atomic distances. At such small volumes the assumption of continuity is of course inaccurate and discrete models must be used.

In the case of metals, under non-uniform plastic deformation fields a size dependent behavior has been observed at scales many times larger than typical dimensions of the Representative Volume Element (RVE) of the material, [1, 2, 3, 4, 5, 6, 7, 8]. Clearly, at such scale the assumption of continuity is still valid provided that the used continuum mechanics model incorporates material length scale parameters. As a result, when some characteristic dimension of the non-uniform plastic deformation field approaches the material length scale, size effects are triggered. The excess of strength identified at the small scale increases in the direction of decreasing specimen size. This behavior has been attributed to an accumulation of an additional dislocation density needed to accommodate the gradients of plastic strain. The proposed models to explain this type of behavior have been termed Strain Gradient Plasticity (SGP) or Geometrically Necessary Dislocations Based Plasticity (GNDP), [9, 10, 11].

1.2 The lack of a length scale

Classical continuum mechanics theories are strongly based on the Cauchy stress principle or Cauchy first postulate and therefore have no internal length scale. They implicitly assume that the wavelength of the imposed deformation field is many times larger than the RVE of the material and in the limiting process that yields to the notion of the classical tractions vector, the ratio between the equivalent surface moments to the surface area vanishes. This means that there is a direct equivalence between the mathematical concept of limit and the physical problem; continuity is therefore assumed accurate regardless of the scale of the problem and gradients of strain are rapidly smoothed out. This lack of internal length scale in classical continuum mechanics theories render the resulting models short of being able to predict the wide range of observed size dependent phenomena related to inelastic behavior.

There are several SGP theories available in the literature, [1, 9, 10, 11, 12, 13, 14, 15] [16], [17], [18] and [19]. In all of them a length scale material parameter (ℓ) appears as an additional mechanical property that enhances the resistance with the gradients of strain. Once the gradients of strain are explicitly considered, additional kinematic variables and stress definitions appear into the formulation.

In the class of theories promulgated in [1], [9] and [15] the gradients of strain appear directly into the governing differential equations giving rise to additional boundary conditions. Similarly, in the models proposed in [12], [13] and [14] the gradients of strain appear indirectly into the yield surface definition, giving rise to a differential equation in the consistency parameter and satisfying the consistency condition only in a weak sense.

1.3 Difficulties in the numerical treatment of strain gradient plasticity theories

Several questions immediately arise if plastic size effects are to be considered: for instance it is not clear how to incorporate gradients of strain into the existing continuum mechanics theories, how to extend the resulting formulations to the inelastic regime and how to extend the available numerical schemes

to the new class of theories. The present article addresses numerical issues related to the last two aspects, namely the proper implementation of strain gradient theories into a finite element scheme and the extension of the model to the inelastic regime.

The explicit consideration of gradients of strain into the continuum which are now needed if one wants to predict size dependent response, immediately demands for higher orders of continuity in the interpolation shape functions used in a finite element implementation. This numerical problem has been generally neglected or addressed empirically based on the fact that experimentally observed results have been correctly predicted. Depending on the type of theory to implement, C^1 (first order continuous) or even superior elements are needed. Generally speaking C^1 or higher order continuous elements are computationally expensive, cumbersome to implement into existing finite element platforms and generally not readily available. Alternatively, one can use C^0 continuous elements and impose the new kinematic variables as kinematic constraints satisfied in a weak sense. This general alternative for the class of gradient theories has not been thoroughly discussed in the literature and the problem has been solved rather empirically.

In the present article we address the problem of how to properly implement a strain gradient theory for the special case of a Cosserat Couple Stress Based Strain Gradient Plasticity Framework, (CS–SGP). We discuss different alternatives for the numerical implementation of the theory giving rise to either a mixed or a hybrid scheme. On the other hand we also present an extension of an existing deformation theory plasticity model with size effects to a flow theory formulation. This overcomes the limitation existing in deformation theories where only proportional loading problems can be studied. The resulting Cosserat continuum mechanics framework is therefore coupled with a rate independent inelastic constitutive model expressed in flow theory form. The Cosserat framework and constitutive model are cast in the form of a user element subroutine UEL and a material user subroutine UMAT which guarantees portability of the algorithm. The algorithm is tested simulating the microbending experiment reported in [7] to verify the model capability to incorporate plastic size effects. The total computational framework is included in the appendix in the form of a resulting Newton-Raphson iteration.

2 The general and reduced cosserat couple stress theory

The description that follows refers to the general solid occupying a volume Ω and bounded by a surface $\partial\Omega$ with outward normal vector $\hat{n}$, figure 1. We will refer to volume differentials as $d\Omega$ and surface area differentials as $d\Gamma$ and will work within a small displacements and small strains context.

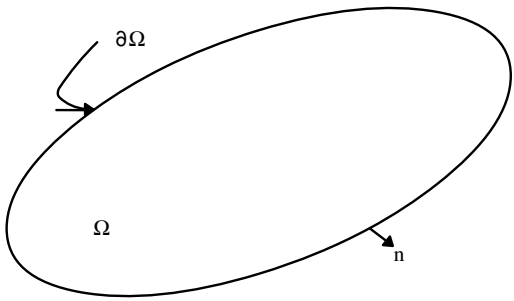

Figure 1: schematic of the assumed general solid

In the couple stress theory described in [20] a differential material element admits not only normal and shear stresses but also couple stress components. This could be interpreted as an extension of the first postulate of Cauchy which immediately leads to a more general definition of the tractions vector. From the kinematics perspective two models were originally formulated by the Cosserats, [20]; both models are presented in the discussion that follows.

2.1 Equilibrium equations, kinematic relations and generalized Hooke's law

For linear elastic behavior the stress components are functions of the strains and the couple stresses are functions of the curvatures. The equations of equilibrium and traction boundary conditions are given in (1) where σ_{ij} represents the symmetric component of the stress tensor, τ_{ij} the asymmetric component of the stress tensor, m_{ij} the couple stress tensor and t_i and q_i represent force and moment tractions respectively

$$\begin{aligned} \sigma_{ji,j} + \tau_{ji,j} &= 0 \\ \tau_{jk} + \frac{1}{2} e_{ijk} m_{pi,p} &= 0 \end{aligned} \tag{1a}$$

$$\begin{aligned} t_i &= (\sigma_{ij} + \tau_{ij}) n_j \\ q_i &= m_{ij} n_j \, . \end{aligned} \tag{1b}$$

In (1), e_{ijk} represents the permutation tensor and n_j the vector normal to the bounding surface $d\Gamma$. From the kinematics point of view two distinct theories are identified in the work of the Cosserats as described by [21], [22] and [23]. First, there is formulated a General Cosserat Couple Stress Theory where within a material point there is also assumed to be embedded a micro–volume. In principle this micro–volume could admit several micro-deformation modes, see [22], [24], [25] and [26]. In the particular case of the Cosserat general theory a material point can sustain, in addition to the usual rotation θ_i which is kinematically constrained to the displacement vector u_i, a micro–rotation ω_i present inside the micro–volume. The material point rotation θ_i and the micro–rotation ω_i are related through a relative rotation tensor α_{ij}. The kinematic relations corresponding to the general theory are described in (2) where $\varepsilon_i j$ represents the small strains tensor, χ_{ij} represents the curvatures (or gradients of the material point rotation).

$$\begin{aligned} \varepsilon_{ij} &= \frac{1}{2} \left(u_{i,j} + u_{j,i} \right) \\ \theta_i &= \frac{1}{2} e_{ijk} u_{k,j} \\ \alpha_{ij} &= e_{ijk} \omega_k - e_{ijk} \theta_k \\ \chi_{ij} &= \theta_{i,j} \, . \end{aligned} \tag{2}$$

The generalized Hooke's law for the Cosserat Couple Stress Solid are presented in (3) where C_{ijkl}, $\bar{D}_{ijkl}$ and D_{ijkl} are constitutive tensors relating the symmetric part of the stress tensor to the strains, the asymmetric part of the stress tensor to the relative rotations and the couple stress tensor to the curvatures via a material length scale parameter ℓ respectively.

$$\begin{aligned} \sigma_{ij} &= C_{ijkl}\varepsilon_{kl} \\ \tau_{ij} &= \bar{D}_{ijkl}\alpha_{kl} \\ \ell^{-1}m_{ij} &= D_{ijkl}\ell\chi_{kl}\,. \end{aligned} \tag{3}$$

Secondly, there is a reduced couple stress theory which corresponds to the particular choice of $\omega_k = \theta_k$. In this case the relative rotation tensor α_{ij} vanishes and the general couple stress theory reduces to the more restrictive reduced couple stress theory. In this reduced theory the kinematic quantities are now the displacement u_i and the associated material rotation θ_i tied to the displacements by the kinematic constraint given in (2). In this case there is still an asymmetric part of the stress tensor which makes a null work upon deformation. Figure 2 shows the particular case of reduced couple stress theory where the micro–volume is assumed rigid or without relative rotations.

2.2 Total potential energy functional and alternatives for finite element implementation

In the present work interest is on the Cosserat reduced couple stress theory. However it is convenient to consider the reduced model as a particularization of the more general theory. Following a variational approach the reduced model can be identified as a constrained version of the general theory. This scheme allows us to identify different versions of the principle of virtual displacements while keeping a physical meaning. In this way we arrive at different variational equations starting from an unrestricted variational problem and ending with the corresponding restricted problem. The restricted problem can be treated either via a Lagrange multipliers approach or with a penalty function formulation.

Consider the total potential energy functional corresponding to the Cosserat general model, equation 4a. For this theory the independent kinematic variables correspond to the displacements u_i and the micro–rotation ω_i.

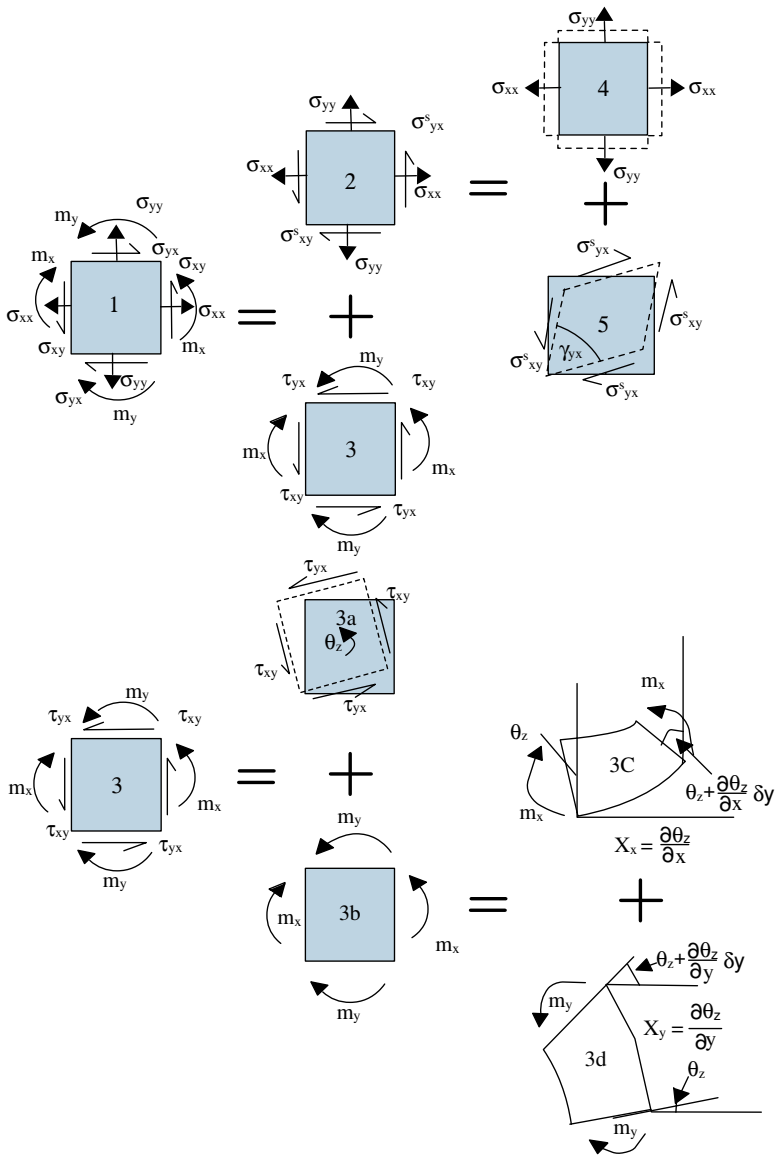

Figure 2: kinematics of the reduced theory couple stress solid

$$\Pi(u_i,\omega_j) = \frac{1}{2}\int_\Omega C_{ijkl}\varepsilon_{kl}(u_i)\varepsilon_{ij}(u_i)d\Omega + \frac{1}{2}\int_\Omega D_{ijkl}\chi_{ij}(\omega_i)\chi_{kl}(\omega_i)d\Omega + \frac{1}{2}\int_\Omega \bar{D}_{ijkl}\alpha_{ij}(u_i,\omega_i)\alpha_{kl}(u_i,\omega_i)d\Omega - \int_{\partial\Omega} t_i u_i d\Gamma - \int_{\partial\Omega} q_i\omega_i d\Gamma\,. \tag{4a}$$

In the case of the reduced theory the independent kinematic variables are only the displacements. The curvatures are then specified as second order gradients of the displacements. The total potential energy functional becomes:

$$\bar{\Pi}(u_i) = \frac{1}{2}\int_\Omega C_{ijkl}\varepsilon_{kl}(u_i)\varepsilon_{ij}(u_i)d\Omega + \frac{1}{2}\int_\Omega D_{ijkl}\chi_{ij}(u_i)\chi_{kl}(u_i)d\Omega - \int_{\partial\Omega} t_i u_i d\Gamma - \int_{\partial\Omega} q_i\omega_i(u_i)d\Gamma\,. \tag{4b}$$

Alternatively, the total potential energy functional for the reduced theory can be written using as independent kinematic variables the displacements and the micro–rotations and imposing the kinematic constraint of vanishing relative rotation somewhere else. In this way it is valid to express the curvatures as first order derivatives of the micro–rotations eliminating the strong continuity requirement in the displacement shape functions in a finite element implementation. This means C^0 elements can still be used. The corresponding functional for the reduced theory is then written like

$$\hat{\Pi}(u_i,\omega_i) = \frac{1}{2}\int_\Omega C_{ijkl}\varepsilon_{kl}(u_i)\varepsilon_{ij}(u_i)d\Omega + \frac{1}{2}\int_\Omega D_{ijkl}\chi_{ij}(\omega_i)\chi_{kl}(\omega_i)d\Omega - \int_{\partial\Omega} t_i u_i d\Gamma - \int_{\partial\Omega} q_i\omega_i d\Gamma\,. \tag{4c}$$

The only difference between the functionals $\bar{\Pi}(u_i)$ and $\hat{\Pi}(u_i,\omega_i)$ corresponding to the reduced theory lies in the assumed independent kinematic variables. It must be clarified that in the one corresponding to (4c) an additional kinematic constraint must be imposed. Following the standard calculus

of variations approach we can arrive at statements corresponding to the Principle of Virtual Work (PVW) for the functionals specified in (4a) to (4c). We present the corresponding principles for completeness and in order to facilitate physical interpretation of the involved terms. In the present work however interest is in the reduced theory.

2.2.1 General Cosserat Couple Stress Solid (Pure displacements). For the general theory the PVW can be directly derived via the first variation of (4a).

$$\int_{\Omega} \sigma_{ij}\varepsilon_{ij}(v_i)d\Omega + \int_{\Omega} m_{ij}\chi_{ij}(\phi_i)d\Omega + \int_{\Omega} \tau_{ij}\alpha_{ij}(v_i,\phi_i)d\Omega - \int_{\partial\Omega} t_i v_i d\Gamma - \int_{\partial\Omega} q_i\phi_i d\Gamma = 0\,. \tag{5a}$$

In (5a) functions v_i, ϕ_i represent virtual quantities (first variations) of real quantities u_i, ω_i. As can be identified from (5a) a finite element implementation of the general theory just requires C^0 continuity in the interpolation function in addition to the independent inclusion of the micro–rotation degree of freedom. In this sense a finite element implementation of the theory is straightforward from the continuity point of view.

2.2.2 Reduced Cosserat Couple Stress Solid (Pure displacements). For the reduced theory the PVW can be directly derived via the first variation of (4b).

$$\int_{\Omega} \sigma_{ij}\varepsilon_{ij}(v_i)d\Omega + \int_{\Omega} m_{ij}\chi_{ij}(v_i)d\Omega - \int_{\partial\Omega} t_i v_i d\Gamma - \int_{\partial\Omega} q_i\phi_i(v_i)d\Gamma = 0\,. \tag{5b}$$

A finite element implementation of the reduced theory based on (5b) demands for C^1 continuity in the shape functions as the curvatures correspond to second order derivatives of the primary displacement function. This is mathematically inconvenient due to the lack of numerically efficient and well studied C^1 elements.

2.2.3 Reduced Cosserat Couple Stress Solid (Lagrange multipliers). Alternatively, the problem can be treated starting from (4c) provided the kinematic constraint is enforced in some sense. This is mathematically and numerically convenient since the continuity requirements are once again C^0 if the curvatures are expressed as gradients of the micro–rotation which appear now as independent kinematic variables. The kinematic constrain can be imposed using a Lagrange multipliers scheme. The corresponding PVW statement is given in (5c).

$$\int_\Omega \sigma_{ij}\varepsilon_{ij}(v_i)d\Omega + \int_\Omega m_{ij}\chi_{ji}(\phi_i)d\Omega - \int_\Omega \tau_{ij}\alpha_{ij}(v_i,\phi_i)d\Omega = \int_{\partial\Omega} t_i v_i d\Gamma + \int_{\partial\Omega} q_i\phi_i d\Gamma \\ \int_\Omega \rho_{ij}\alpha_{ij}(u_i,\omega_i)d\Omega = 0\,. \tag{5c}$$

In (5c) it is possible to identify the Lagrange multiplier ρ_{ij} with the asymmetric part of the stress tensor. This statement could be used for a finite element implementation of the reduced theory, but special attention must be given to the resulting stiffness matrix at the global level. This illed numerical behavior is typical of all mixed formulations which may be problematic if the element is to be implemented in a platform that restricts access to the global stiffness matrix. The present mixed approach is completely equivalent to the one available in [27] and has also been used in [28] and [29].

2.2.4 Reduced Cosserat Couple Stress Solid (Penalty function). The approach followed in 2.2.3 can also be followed but imposing the kinematic constraint using a penalty function approach. This strategy has the advantage that the number of degrees of freedom in a FE formulation remains the same and the resulting matrices can be assembled following standard procedures. The corresponding PVW is given in (5d).

$$\int_\Omega \sigma_{ij}\varepsilon_{ij}(v_i)d\Omega + \int_\Omega m_{ij}\chi_{ij}(\phi_i)d\Omega + \int_\Omega G\alpha_{ij}\alpha_{ij}(v_i,\phi_i)d\Omega - \\ \int_{\partial\Omega} t_i v_i d\Gamma - \int_{\partial\Omega} q_i\phi_i d\Gamma = 0\,. \tag{5d}$$

In (5d) the term $G\alpha_{ij}$ also corresponds to the asymmetric component of the stress tensor, but now the constrain is being imposed through the penalty

parameter G. The advantage is clearly identified in the fact that the theory can now be formulated with a C^0 continuous element. Xia and Hutchinson [30] used (5d) with degrees of freedom being the displacements and displacements derivatives. In that particular implementation the kinematic constrain between displacements and rotations was not enforced, therefore leading to expected pathological mesh dependencies. Wei and Hutchinson [31] used (5d) with degrees of freedom being only the translational components of displacement and with C^0 continuous interpolation functions in a clear violation of the continuity conditions demanded by the finite element method. Begley and Hutchinson [32] used the higher order equivalent of (5d) where displacement and displacement derivatives were considered as nodal degrees of freedom, again with no enforcement of the kinematic constrain. This approach guarantees C^1 continuity only at the nodes and not along the complete inter–element boundaries analogously to the elements by [30]. The following section describes the details of the implementation of the reduced theory using (5d).

2.3 Finite element discretization of the Reduced Couple Stress Theory–Penalty based/reduced integration approach

This section presents the discretized version of the equations corresponding to the BVP formulated in (1)–(3) and starting from the constraint variational problem with corresponding PVW formulated in (5d). The resulting element can be straightforwardly implemented in standard finite element platforms allowing user element subroutines. It only requires the formulation of the local stiffness matrix. In the present work the resulting element has been implemented as a user element subroutine UEL into the commercial code ABAQUS. Letting $\hat{\bar{u}}_e^T = [u_1 v_1 \omega_1 \dots u_n v_n \omega_n]$ correspond to the nodal point displacements vector for a n–noded element we have the following discrete version of (5d):

$$\left[\int_{\Omega_e} B_E^T M B_E dV + G_a \int_{\Omega_e} B_\alpha^T B_\alpha dV \right] \hat{\bar{u}}_e = \int_{\partial\Omega_e} N^T \bar{t} dS + \int_{\partial\Omega_e} B_\alpha^T \bar{q} dS \,. \qquad (6)$$

Equation (6) can be understood as follows. Starting from (5d), σ_{ij} and $\ell^{-1} m_{ij}$ and ε_{ij} and $\ell \chi_{ij}$ have been collapsed into generalized stresses Σ and

generalized strains E respectively. These generalized variables are then related by a generalized constitutive elasticity matrix M collecting the tensors C and D and leading to the generalized form of Hooke´s law.

$$\Sigma = ME \equiv \begin{bmatrix} C & 0 \\ 0 & D \end{bmatrix} \begin{bmatrix} \varepsilon \\ l\chi \end{bmatrix}. \tag{7a}$$

Similarly, t_i and q_i in (5d) have been collapsed into a single tractions vector $\bar{t}$ and the general displacement vector including translational and rotational degrees of freedom into a single displacement vector $\bar{u}$.

The displacements at any point of a n–noded finite element are then interpolated from the nodal point displacements in the standard form

$$\begin{bmatrix} u_e \\ \omega_e \end{bmatrix} = \begin{bmatrix} N_u^1, 0, N_u^2, \ldots, N_u^N, 0 \\ 0, N_\omega^1, 0, \ldots, 0, N_\omega^N \end{bmatrix} \begin{bmatrix} \hat{u}_e \\ \hat{\omega}_e \end{bmatrix} \equiv \bar{u}_e = N\hat{\bar{u}}_e\,, \tag{7b}$$

where $\hat{u}_e$ and ω_e are translational and rotational nodal degrees of freedom as shown in figure 3 and N_u^i, N_ω^i are displacement interpolation functions.

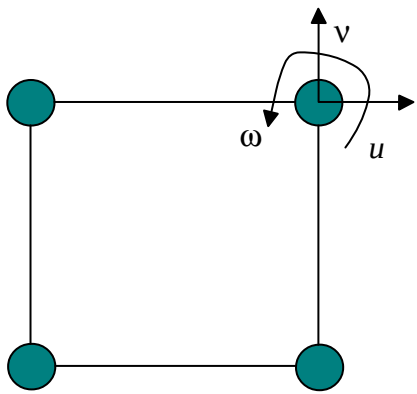

Figure 3: typical finite element for the case of reduced couple stress theory using penalty based approach

In similar form the generalized strain can be obtained by introducing a generalized strain–displacement operator

$$B_E = \begin{bmatrix} B_\varepsilon \\ B_\chi \end{bmatrix} = \begin{bmatrix} \partial/\partial x & 0 & 0 \\ 0 & \partial/\partial y & 0 \\ 0 & 0 & 0 \\ \partial/\partial y & \partial/\partial x & 0 \\ 0 & 0 & \ell\partial/\partial x \\ 0 & 0 & \ell\partial/\partial y \end{bmatrix}, \tag{7c}$$

then $E = B_E \hat{\hat{u}}_e$. Similarly the constraint operator B_α is introduced and such $\alpha = B_\alpha \hat{\hat{u}}_e$ and (6) then follows directly from substitution of (7a) through (7d) in (5d).

$$B_\alpha = \frac{1}{2}\begin{bmatrix} \partial/\partial y & -\partial/\partial x & N \end{bmatrix}. \tag{7d}$$

Making explicit the contribution from the translational and rotational degrees of freedom (6) can be written as

$$\left\{ \begin{bmatrix} K_{uu} & 0 \\ 0 & K_{\omega\omega} \end{bmatrix} + \begin{bmatrix} K^\lambda_{uu} & K^\lambda_{u\omega} \\ K^\lambda_{\omega u} & K^\lambda_{\omega\omega} \end{bmatrix} \right\} \begin{bmatrix} \hat{u}_e \\ \hat{\omega}_e \end{bmatrix} = \begin{bmatrix} f_u \\ f_\omega \end{bmatrix}. \tag{8}$$

In (8) the second matrix corresponds to the contribution from the penalty terms and the following limits should be identified. As $G_a \to \infty$ the formulation approaches the reduced couple stress theory. If $\ell \to 0$ and $G_a \to \infty$ then the formulation approaches classical theory. Here classical theory means a solid with translational and rotational degrees of freedom with the kinematic constrain expressed in (2) enforced by the penalty term and with no contribution from the couple stress terms. Notice that if in (8) both $\ell \to 0$ and $G_a \to \infty$ simultaneously, then the constrain established in (2) is violated and the stiffness matrix becomes singular. In (8) the first term in the left hand side is fully integrated whereas the second term depending on the penalty number G_a is integrated using a reduced scheme.

2.4 Cosserat couple stress based strain gradient plasticity theory

The continuum model described in the previous section is extended here to incorporate gradient effects due to non–uniform plastic deformation fields.

This implies the generalization of the stress space to include couple stresses. In this way the yield surface is considered a sphere in an extended stress space where the classical theory solid represents just a subset of the more general model. The gradient effects are then introduced by enhancing the definition of equivalent plastic strain with the addition of an equivalent plastic curvature. This approach leads to a straightforward extension of the flow theory description used in a classical solid which allows the treatment of cyclic loading problems as in the case of low cycle fatigue analysis.

The formulation that follows presents the continuum flow theory equations for a rate independent material under the assumption of small displacements and small strains. A key feature in the formulation is the coupling between the symmetric part of the stress tensor and the Couple stresses. This coupling is not present in the initial elastic material model, see (3), but progressively develops with the appearance of the plastic curvatures as becomes evident in the continuous version of the elasto–plastic material Jacobian. The proposed constitutive model was integrated using a radial return scheme. The integration algorithm was implemented into an ABAQUS material user subroutine UMAT which is at the same time invoked by the element user subroutine UEL with formulation proposed in sections 2.2.4 and 2.3.

2.4.1 Rate independent non–linear material behavior. Recalling the relationship between the symmetric part of the stress tensor and the elastic strains and the couple stresses and the elastic curvatures first presented in (3), they can be written in rate form as

$$\begin{aligned} \dot{\sigma}_{ij} &= C_{ijkl}\dot{\varepsilon}^{el}_{kl} \\ \ell^{-1}\dot{m}_{ij} &= D_{ijkl}\ell\dot{\chi}^{el}_{kl}\,. \end{aligned} \tag{9}$$

The strains and curvatures are now decoupled into elastic and inelastic components which results in

$$\begin{aligned} \dot{\varepsilon}_{ij} &= \dot{\varepsilon}^{el}_{ij} + \dot{\varepsilon}^{pl}_{ij} \\ \ell\dot{\chi}_{ij} &= \ell\dot{\chi}^{el}_{ij} + \ell\dot{\chi}^{pl}_{ij}\,. \end{aligned} \tag{10}$$

Consider now the following definition of the generalized deviatoric stress norm $\| \Sigma' \|$

$$\| \Sigma' \| = [S_{ij}S_{ij} + \ell^{-1}m_{ij}\ell^{-1}m_{ij}]^{\frac{1}{2}}\,, \tag{11}$$

where S_{ij} is the symmetric deviatoric component of σ_{ij} and the anti–symmetric tensor m_{ij} is deviatoric in nature. Similarly, we have for the generalized strain where ε_{ij} and χ_{ij} are symmetric and anti–symmetric respectively thus leading to the following norm for the combined tensor

$$\| E \| = [\varepsilon_{ij}\varepsilon_{ij} + \ell\chi_{ij}\ell\chi_{ij}]^{\frac{1}{2}} . \tag{12}$$

Next we introduce a yield surface separating the elastic and inelastic domains and in an analogous way to the classical Hill plasticity models. In order to consider the Bauschinger effect observed in metals and its alloys, a back–stress tensor β_{ij} and a couple back–stress tensors $\ell^{-1}\eta_{ij}$ defining the displacement of the yield surface in stress space can also be defined. The assumption of the presence of the couple back–stress tensor is motivated theoretically and not based on any experimental evidence. The difference $f_{ij} = S_{ij} - \beta_{ij}$ between the back–stress and the deviatoric component of the symmetric part of the Cauchy stress tensor is the relative stress tensor f_{ij}. In an analogous form for the couple back–stress, there follows that the relative couple back–stress $\ell^{-1}\hat{C}_{ij}$ is defined by $\ell^{-1}\hat{C}_{ij} = \ell^{-1}m_{ij} - \ell^{-1}\eta_{ij}$. The generalized relative stress $\| \xi \|$ can be described in terms of the relative stresses and given by

$$\| \vec{\xi} \| = [f_{ij}f_{ij} + \ell^{-2}\hat{C}_{ij}\hat{C}_{ij}]^{\frac{1}{2}}. \tag{13}$$

With (13) at hand a yield surface is introduced. In the classical theory of plasticity the yield surface is defined in terms of a hardening parameter that can be shown to be proportional to the equivalent plastic strain. In the present couple stress based strain gradient plasticity theory this hardening parameter incorporates also the gradient effects via the equivalent plastic curvatures. The generalized yield surface can therefore be expressed as

$$F(\sigma, \ell^{-1}m, \alpha) = \| \xi \| - \sqrt{\frac{2}{3}}K(\alpha) , \tag{14}$$

where α is the generalized hardening parameter and $K(\alpha)$ represents the radius of the yield surface in the enhanced stress space. In order to complete the description of the flow theory representation of the constitutive model, it is necessary to define the flow rules (i.e., evolution equations for the plastic strains and curvatures) and hardening laws (i.e., evolution of the hardening

parameter and back–stress components). Here it is assumed that the flow rules obey associative normal plasticity rules. To this end, it is necessary to define the normal to the yield surface as in [9]. Notice that the generalization implied in (14) amounts to considering a more general stress space with normal and couple stresses. Thus the yield surface is still considered as an hyper–sphere in stress space with normal defined by (15),

$$\underline{\hat{N}} = \frac{\partial F}{\partial \vec{\Sigma}} \equiv [\underline{\hat{n}}, \underline{\hat{v}}]\,, \tag{15}$$

where $\underline{\hat{n}}_{ij} = \frac{\partial F}{\partial \sigma_{ij}} \equiv \frac{f_{ij}}{\|\xi_{ij}\|}$ and $\underline{\hat{v}}_{ij} = \frac{\partial F}{\partial \ell^{-1} m_{ij}} \equiv \ell^{-1} \frac{\hat{C}_{ij}}{\|\xi_{ij}\|}$.

The flow rules read

$$\dot{\varepsilon}^{pl}_{ij} = \gamma \frac{\partial F}{\partial \sigma_{ij}} \equiv \gamma \frac{f_{ij}}{\| \xi_{ij} \|} \equiv \gamma \underline{\hat{n}}_{ij}\,, \tag{16a}$$

$$\ell \dot{\chi}^{pl}_{ij} = \gamma \frac{\partial F}{\partial \ell^{-1} m_{ij}} \equiv \gamma \ell^{-1} \frac{\hat{C}_{ij}}{\| \xi_{ij} \|} \equiv \gamma \underline{\hat{v}}_{ij}\,. \tag{16b}$$

In (16) γ is the consistency parameter which is defined from the loading/unloading conditions and is related to the evolution of the generalized equivalent plastic strain defined by the hardening law established in (17).

$$\dot{\alpha} = \sqrt{\frac{2}{3}} \gamma\,. \tag{17}$$

The constitutive model is completed with the evolution equations for the back–stresses

$$\dot{\beta}_{ij} = \frac{2}{3} H' \gamma \underline{\hat{n}}_{ij}\,, \tag{18a}$$

$$\ell \dot{\eta}_{ij} = \frac{2}{3} H' \gamma \underline{\hat{v}}_{ij}\,, \tag{18b}$$

where H' represents a kinematic hardening modulus which may be a linear or a nonlinear function of the hardening parameter α. For instance, the assumption of a constant kinematic hardening modulus leads to the so–called Prager–Ziegler rule, [34]. Using (18) into the generalized strain norm for the plastic quantities yields

$$\| \dot{E}^{pl} \| = \left[\dot{\varepsilon}^{pl}_{ij} \dot{\varepsilon}^{pl}_{ij} + \ell^2 \dot{\chi}^{pl}_{ij} \dot{\chi}^{pl}_{ij} \right]^{\frac{1}{2}} \equiv \frac{\gamma}{\| \xi_{ij} \|} \left[f_{ij} f_{ij} + \ell^{-2} \hat{C}_{ij} \hat{C}_{ij} \right]^{\frac{1}{2}},$$

which implies $\| \dot{E}^{pl} \| = \gamma$.

Using this result in (17) and integrating we have the following generalized version of equivalent plastic strain but with the addition of the gradients of plastic strain.

$$\alpha(t) = \int_0^t \sqrt{\frac{1}{2}} \| \dot{E}^{pl}(\tau) \| \, d\tau \,. \tag{19}$$

The evolution equations are complemented by the loading/unloading conditions which allow the determination of the consistency parameter. In terms of the yield function defined in (14) the following loading/unloading condition holds

$$\gamma \geqslant 0 \quad F(\sigma, \ell^{-1} m, \alpha) \leqslant 0 \,, \tag{20a}$$

$$\gamma \geqslant 0 \quad \gamma F(\sigma, \ell^{-1} m, \alpha) = 0 \,. \tag{20b}$$

And the consistency condition

$$\gamma \dot{F}(\sigma, \ell^{-1} m, \alpha) = 0 \,. \tag{21}$$

From the definition of the yield function and the consistency condition the consistency parameter can be determined

$$\gamma = \frac{1}{\| \Sigma \|} \frac{S : \dot{\varepsilon} + \ell^{-1} : \ell \dot{\chi}}{\left(1 + \frac{K'}{3\mu} \right)} = \frac{1}{\| \Sigma \|} \frac{S : \dot{\varepsilon} + \ell^{-1} : \ell \dot{\chi}}{\hat{K}} \,. \tag{22}$$

Using this result into Hooke's law yields

$$\dot{\sigma} = C : \dot{\varepsilon} - \frac{2\mu}{\hat{K}} (\hat{\underline{n}} \otimes \hat{\underline{n}}) : \dot{\varepsilon} - \frac{2\mu}{\hat{K}} (\hat{\underline{n}} \otimes \hat{\underline{v}}) : \ell \dot{\chi} \,, \tag{23a}$$

$$\ell^{-1} \dot{m} = D : \ell \dot{\chi} - \frac{2\mu}{\hat{K}} (\hat{\underline{n}} \otimes \hat{\underline{v}}) : \dot{\varepsilon} - \frac{2\mu}{\hat{K}} (\hat{\underline{v}} \otimes \hat{\underline{v}}) : \ell \dot{\chi} \,. \tag{23b}$$

Using $C = \kappa \hat{I} \otimes \hat{I} + 2\mu \left(\hat{\coprod} - \frac{1}{3} \hat{I} \otimes \hat{I} \right)$ and $D = 2\mu \hat{\coprod}$ and after simplifying yields

$$M^{ep} = \begin{pmatrix} \kappa \hat{I} \otimes \hat{I} + 2\mu \left(\hat{\coprod} - \frac{1}{3} \hat{I} \otimes \hat{I} - \frac{\hat{\underline{n}} \otimes \hat{\underline{n}}}{\hat{K}} \right) & -2\mu \frac{\hat{\underline{n}} \otimes \hat{\underline{v}}}{\hat{K}} \\ -2\mu \frac{\hat{\underline{n}} \otimes \hat{\underline{v}}}{\hat{K}} & 2\mu \left(\hat{\coprod} - \frac{\hat{\underline{v}} \otimes \hat{\underline{v}}}{\hat{K}} \right) \end{pmatrix} . \tag{24}$$

Alternatively it can be written

$$M^{ep} = \begin{bmatrix} C - C : \frac{\hat{\underline{n}} \otimes C : \hat{\underline{n}}}{\hat{K}} & -C : \frac{\hat{\underline{n}} \otimes D : \hat{\underline{v}}}{\hat{K}} \\ -D : \frac{\hat{\underline{v}} \otimes C : \hat{\underline{n}}}{\hat{K}} & D - D : \frac{\hat{\underline{v}} \otimes D : \hat{\underline{v}}}{\hat{K}} \end{bmatrix} . \tag{25}$$

Equations (23) can be written in compact form like

$$\dot{\Sigma} = \left[M - \frac{2\mu}{\hat{K}} \left(\hat{\underline{N}} \otimes \hat{\underline{N}} \right) \right] : \dot{E} . \tag{26}$$

The constitutive tensor given by (26) is equivalent to the one in (23). It can be seen from (23) that the coupling between strains and curvatures becomes evident in the off–diagonal terms in the generalized constitutive tensor. The discrete version of the material Jacobian (25) after using a radial return algorithm is presented below.

$$M^{ep}_{n+1} = \begin{bmatrix} \kappa \hat{I} \otimes \hat{I} + 2\mu\delta_{n+1} \left(\hat{\coprod} - \frac{1}{3} \hat{I} \otimes \hat{I} \right) - 2\mu\overline{\theta}_{n+1} \hat{\underline{n}}_{n+1} \otimes \hat{\underline{n}}_{n+1} & -\frac{2\mu}{\hat{K}} \hat{\underline{n}}_{n+1} \otimes \hat{\underline{v}}_{n+1} \\ -\frac{2\mu}{\hat{K}} \hat{\underline{n}}_{n+1} \otimes \hat{\underline{v}}_{n+1} & 2\mu\delta_{n+1} \hat{\coprod} - 2\mu\overline{\theta}_{n+1} \underline{v}_{n+1} \otimes \hat{\underline{v}}_{n+1} \end{bmatrix} , \tag{27}$$

when $\delta t \to 0$ (27) tends to (25). The coupling between the curvatures and strains apparent in the continuous version of the tangent stiffness matrix is again evident in the algorithmic version as can be seen from (27).

3 Numerical validation–simulation of the microbending experiment

The computational framework proposed in the present article is validated against the results corresponding to the microbending experiments reported

in [7] and [8]. In both experiments the loads are applied monotonically and the material is assumed to exhibit rate independent behavior. The material properties, including the values of the length scale parameter ℓ correspond to the ones reported in the original papers. The thickness of the micro–beams in [7] correspond to 12.5 μm, 25.0 μm and 50.0 μm and those in [8] correspond to 25.0 μm and 50.0 μm, 100.0 μm and 150.0 μm. For the 100.0 μm and 150.0 μm specimens the gradient effects vanish and are not included here. The material parameters corresponding to both tests are reported in table (1). As reported by the authors constant values of the length scale have been used. A non–constant value of the length scale parameter evolving as a function of the ratio of the grain size to the characteristic specimen dimension has been proposed by [33]. This evolving length scale may improve the fitting to the reported experimental results.

Table 1: material parameters–microbending test simulation

Stolken and Evans(1998)		
Beam thickness(μm)	Σ_0 (Mpa)	E_p(GPa)
12.50	56.00	1.15
25.00	75.00	1.30
50.00	103.00	1.05
Shrotriya et al(2003)		
25.00	400.00	1.03
50.00	400.00	1.03

In the simulations a point load was statically applied at the tip of the different micro–beams in order to achieve a specified moment. Figures 4 and 5 show the experimental and numerical simulation results for both tests. In figure 4, which corresponds to the results reported in [7], the normalized moment $\frac{4M}{\Sigma_0 bt^2}$ is meaningful within the strain gradient plasticity theory reported in [9]. In both simulations the used length scale parameters are $\ell = 5.0\,\mu$m and $\ell = 5.6\,\mu$m. The simulation results and those reported in [7] are in very good agreement. In the experiments a similar strain hardening for the three foils is observed. This trend has been directly included in the simulation where the used isotropic hardening regime is also linear. However this is not the case for the simulations results shown in figure 5 of the test performed

in [8] where apparently there is a nonlinear strain hardening behavior. Since there are no parameters reported by the authors to consider this non–linear effect the numerical predictions remain also linear. This difference is also observed when comparing the experimental results from both authors as can be seen from figure 6. Figure 7 shows computational results for the test reported in [7] using a value of $\ell = 0.0\,\mu$m which correspond to classical theory. In the same figure the corresponding experimental results are also shown for comparison.

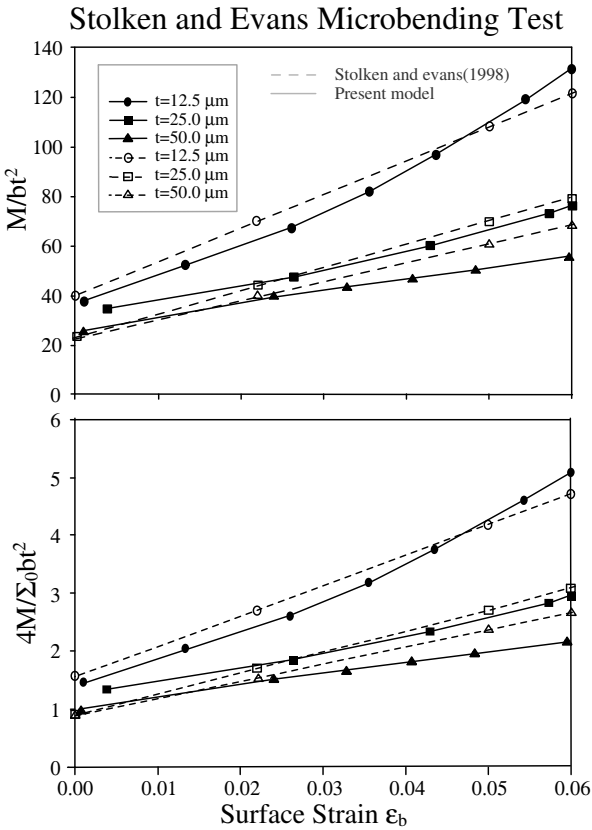

Figure 4: Stolken and Evans(1998). Microbending experimental results on nickel foils compared to present model. $\ell = 5.0\,\mu$m, $E = 220.0$ GPa, $\Sigma_{0(12.5\,\mu\text{m})} = 56.0$ MPa, $\Sigma_{0(25.0\,\mu\text{m})} = 75.0$ MPa, $\Sigma_{0(50.0\,\mu\text{m})} = 103$ MPa

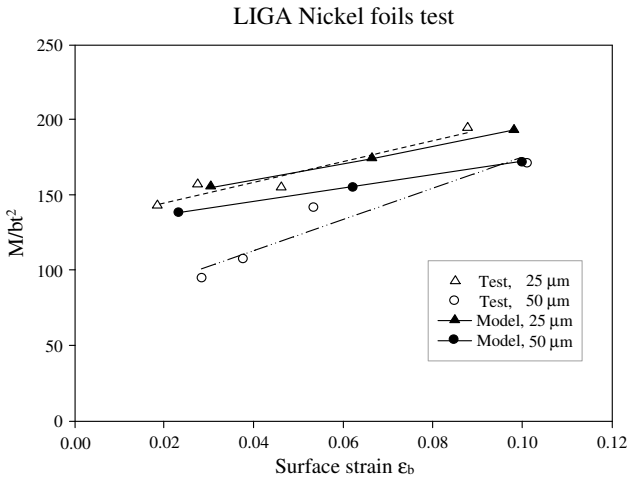

Figure 5: Shrotriya et al(2003). Microbending experimental results on LIGA nickel foils compared to present model. $\ell = 5.6\,\mu$m, $E = 165.0$ GPa, $\Sigma_0 = 400$ MPa

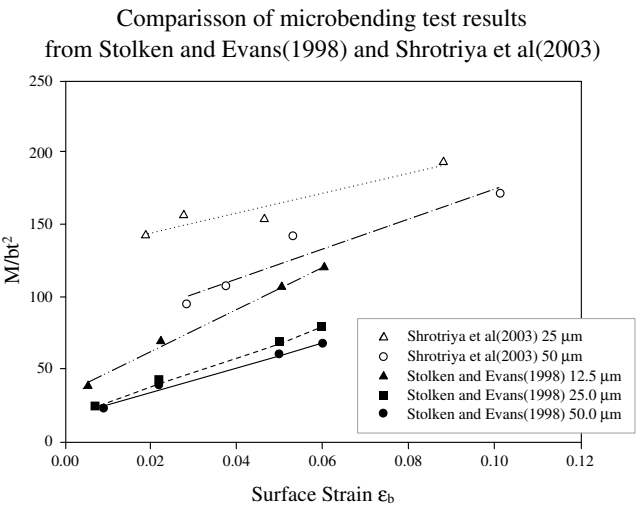

Figure 6: experimental results from the microbending tests on LIGA–nickel foils and pure nickel foils from Shrotriya et al(2003) and Stolken and Evans(1998)

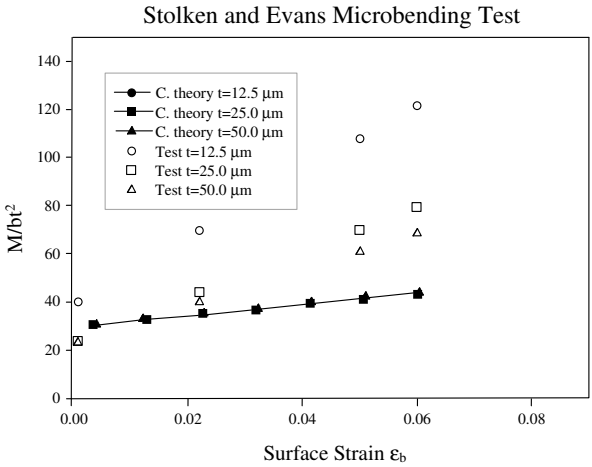

Figure 7: analysis of Stolken and Evans(1998). Specimens using a classical plasticity theory model. The classical theory results are compared against experimental results. $\ell = 0.0\,\mu$m, $E = 220.0$ GPa, $\Sigma_{0(12.5\,\mu\text{m})} = 56.0$ MPa, $\Sigma_{0(25.0\,\mu\text{m})} = 75.0$ MPa, $\Sigma_{0(50.0\,\mu\text{m})} = 103$ MPa

4 Conclusions

The numerical treatment of a commonly used strain gradient plasticity model, namely the Cosserat couple stress theory, has been discussed. Two main issues are identified from a numerical point of view. First is the need for higher order continuity requirements on the interpolation shape functions which is demanded by the presence of the gradients of plastic strain. Second is the need for an integration algorithm when the theory is casted in its rate independent flow theory form. To study the first problem the theory has been placed into a variational approach. As a result different alternatives for the finite element formulation of the problem become available. Although some of these different alternatives have been previously used by other authors we have placed them here within a unified mathematical framework. In particular we have implemented the reduced Cosserat couple stress theory in the form of a reduced integration/penalty function scheme into a user element in the commercial finite element code ABAQUS. The Cosserat theory has been further extended to consider nonlinear material behavior. The equations for

the case of a rate independent material have been presented in its flow theory form. It is clear that once plastic behavior takes place there is coupling between the normal stresses and the couple stress quantities. The rate independent constitutive model has been complemented with an integration algorithm thus allowing its implementation in the user element subroutine UEL. In order to validate the implementation we have used the microbending test in thin nickel foils reported in [7] and [8]. Comparisons between the simulations and the experimental results show general good agreement.

5 Appendix

5.1 Newton–raphson iteration in ABAQUS (UEL)

Let $T \leftarrow 0(time)$

1. Assume ${}^{t}u, {}^{t}E, {}^{t}\Sigma, {}^{t}\kappa$ known
2. Assemble ${}^{t+\Delta t}F_{ext} = \int\limits_{S} N^{T}\, {}^{t+\Delta t}\bar{t} dS$

Initialize ${}^{t+\Delta t}u^{(0)} \leftarrow {}^{t}u$ and ${}^{t+\Delta t}E^{(0)} \leftarrow {}^{t}E$
Let $i \leftarrow 0$, $Flag \leftarrow 0$
Do_While $Flag = 0$

$i \leftarrow i + 1$

(ABAQUS calls user subroutine UEL.f)

Assemble B_E, B_α

Call UMAT.f to compute

$$ {}^{t+\Delta t}\Sigma^{(i-1)},\ {}^{t+\Delta t}\kappa^{(i-1)},\ {}^{t+\Delta t}C^{(i-1)},\ {}^{t+\Delta t}D^{(i-1)} $$

Assemble ${}^{t+\Delta t}K^{(i-1)}$

Assemble residual (RHS)

$$ {}^{t+\Delta t}F^{(i-1)} \leftarrow {}^{t+\Delta t}F_{ext} - \int\limits_{V} B_E^{T}\, {}^{t+\Delta t}\Sigma^{(i-1)} dV - \int\limits_{V} B_\alpha^{T}\, {}^{t+\Delta t}\tau^{(i-1)} dV $$

(Exits user subroutine UEL.f and returns to ABAQUS)

Solve ${}^{t+\Delta t}K^{(i-1)}\Delta u^{(i)} = {}^{t+\Delta t}F^{(i-1)}$

Update

$$
\begin{aligned}
{}^{t+\Delta t}u^{(i)} &\leftarrow {}^{t+\Delta t}u^{(i-1)} + \Delta u^{(i)} \\
{}^{t+\Delta t}E^{(i)} &\leftarrow B\,{}^{t+\Delta t}E^{(i)}
\end{aligned}
$$

If $\|error\| < tol$ **Then** $Flag \leftarrow 1$

End_Do_While

Let $T \leftarrow T + \Delta T$

If $T < T_{\max}$ **Then Goto step 2**

Analysis Complete

5.2 Algorithm for UMAT subroutine

Assume a trial state and Solve for the consistency parameter

$$\Sigma_{n+1}^{tr} = \Sigma_n + 2\mu\Delta E_{n+1}$$

$$\Sigma_{n+1} = \Sigma_{n+1}^{tr} - 2\mu\Delta\gamma\hat{N}_{n+1}$$

$$\hat{N}_{n+1} = \frac{\Sigma_{n+1}^{tr}}{\|\Sigma_{n+1}^{tr}\|}$$

$$\| \Sigma_{n+1}^{tr} \| - \sqrt{\tfrac{2}{3}}K(\alpha_n) - \tfrac{2}{3}K'\Delta\gamma - 2\mu\Delta\gamma = 0$$

$$\Delta\gamma = \frac{F_{n+1}^{tr}}{2\mu\hat{K}}$$

Obtain linearized jacobian

$$\dot{\Sigma}_{n+1} = M : \dot{E}_{n+1} - 2\mu\Delta\gamma\hat{N}_{n+1}$$

$$\frac{d\Sigma_{n+1}}{dE_{n+1}} = M - 2\mu\left[\hat{N}_{n+1} \otimes \frac{d\Delta\gamma}{dE_{n+1}} + \Delta\gamma\frac{d\hat{N}_{n+1}}{dE_{n+1}}\right]$$

$$\frac{d\Delta\gamma}{dE_{n+1}} = \frac{1}{\hat{K}}\hat{N}_{n+1}$$

$$\frac{d\hat{\underline{N}}_{n+1}}{dE_{n+1}} = \frac{2\mu}{\|\Sigma^{tr}_{n+1}\|} H_{n+1}$$

$$H_{n+1} = \begin{bmatrix} \hat{\coprod} - \frac{1}{3}\hat{I} \otimes \hat{I} - \hat{\underline{n}}_{n+1} \otimes \hat{\underline{n}}_{n+1} & 0 \\ 0 & \hat{\coprod} - \hat{\underline{v}}_{n+1} \otimes \hat{\underline{v}}_{n+1} \end{bmatrix}$$

$$\frac{d\Sigma_{n+1}}{dE_{n+1}} = M - 2\mu \left[\frac{\hat{\underline{N}}_{n+1} \otimes \hat{\underline{N}}_{n+1}}{\hat{K}} + \frac{\Delta\gamma 2\mu}{||\Sigma^{tr}_{n+1}||} H_{n+1} \right]$$

$$M^{ep}_{n+1} = \begin{bmatrix} \kappa \hat{I} \otimes \hat{I} + 2\mu\delta_{n+1}\left(\hat{\coprod} - \frac{1}{3}\hat{I} \otimes \hat{I}\right) - 2\mu\bar{\theta}_{n+1}\hat{\underline{n}}_{n+1} \otimes \hat{\underline{n}}_{n+1} & -\frac{2\mu}{\hat{K}}\hat{\underline{n}}_{n+1} \otimes \hat{\underline{v}}_{n+1} \\ -\frac{2\mu}{\hat{K}}\hat{\underline{n}}_{n+1} \otimes \hat{\underline{v}}_{n+1} & -2\mu\delta_{n+1}\hat{\coprod} - 2\mu\bar{\theta}_{n+1}\underline{v}_{n+1} \otimes \hat{\underline{v}}_{n+1} \end{bmatrix}$$

References

[1] N. A. Fleck and J. W. Hutchinson. *A Phenomenological Theory for Strain Gradient Effects in Plasticity*. Journal of the Mechanics and Physics of Solids, ISSN 0022–5096, **41**(12), 1825–1857 (1993). Referenciado en 101, 102

[2] N. A. Stelmashenko, M. G. Walls, L. M. Brown and Yu V. Milman. *Microindentations on W and Mo oriented single crystals : an STM study*. Acta Metallurgica et Materialia, ISSN 1359–6462, **41**(10), 2855–2865 (1993). Referenciado en 101

[3] Qing Ma and David R. Clarke. *Size dependent hardness of silver single crystals*. Journal of Materials Research, ISSN 0884-2914, **10**(4), 853–863 (1995). Referenciado en 101

[4] W. J. Poole, M. F. Ashby and N. A. Fleck. *Micro–hardness of annealed and work-hardened copper polycrystals*. Scripta Mettallurgica et Materialia, ISSN 1359–6462, **34**(4), 559–564 (1996). Referenciado en 101

[5] Ranjana Saha, XueZhenyu, Huang Young and William Nix. *Indentation of a soft metal film on a hard substrate: strain gradient hardening effects*. Journal of the mechanics and physics of solids, ISSN 0022–5096, **49**(9), 1997–2014 (2001). 101

[6] A. A. Elmustafa and D. S. Stone. *Indentation size effect in polycrystalline F. C. C. metals*. Acta Materialia, ISSN 1359–6454, **50**(14), 3641–3650 (2002). Referenciado en 101

[7] J. S. Stölken and A. G. Evans. *A microbend test method for measuring the plasticity length scale*. Acta Materialia, ISSN 1359–6462, **46**(14), 5109–5115 (1998). Referenciado en 101, 103, 119, 120, 123

[8] P. Shrotriya, S. M. Allameh, J. Lou, T. Buchheit and W. O. Soboyejo. *On the measurement of the plasticity length scale parameter in LIGA nickel foils*. Mechanics of materials, ISSN 0167–6636, **35**(3–6), 233–243 (2003). Referenciado en 101, 119, 120, 123

[9] N. Fleck and John W. Hutchinson. *Strain Gradient Plasticity* in Advances in Applied mechanics, John W. Hutchinson and Theodore Y. Wu (Series Editors), ISBN 0120020335, **33**, 295–361 (1997). Referenciado en 101, 102, 116, 119

[10] H. Gao, Y. Huang and W. D. Nix. *Modeling Plasticity at the Micrometer Scale*. Naturwissenschaften, ISSN 0028–1042, **86**(11), 507–515 (1999). Referenciado en 101, 102

[11] H. Gao, Y. Huang, W. D. Nix and J. W. Hutchinson. *Mechanism–based strain gradient plasticity: I Theory*. Journal of the mechanics and physics of solids, ISSN 0022–5096, **47**(6), 1239–1263 (1999). Referenciado en 101, 102

[12] Zdenek P. Bazant. *Size Effect in Blunt Fracture: Concrete, Rock, Metal*. Journal of Engineering Mechanics, ISSN 0733–9399, **110**(4), 518–535 (1984). Referenciado en 102

[13] E. C. Aifantis. *On the role of gradients in the localization of deformation and fracture*. International Journal of Engineering Science, ISSN 0020–7225, **30**(10), 1279–1299 (1992). Referenciado en 102

[14] R. De Borst and H. Mühlhaus. *Gradient–dependent plasticity: formulation and algorithmic aspects*. International journal for numerical methods in engineering, ISSN 0029–5981, **35**(3), 521–539 (1992). Referenciado en 102

[15] N. A. Fleck, G. M. Muller, M. F. Ashby and J. W. Hutchinson. *Strain gradient plasticity: theory and experiment*. Acta metallurgica et materialia, ISSN 0956-7151, **42**(2), 475–487 (1994). Referenciado en 102

[16] Y. Guo, Y. Huang, H. Gao, Z. Zhuang and K. C. Hwang. *Taylor–based nonlocal theory of plasticity: numerical studies of the micro-indentation experiments and crack tip fields*. International journal of solids and structures, ISSN 0020–7683, **38**(42), 7447–7460 (2001). 102

[17] J. L. Bassani. *Incompatibility and a simple gradient theory of plasticity*. Journal of the mechanics and physics of solids, ISSN 0022–5096, **49**(9), 1983–1996 (2001). Referenciado en 102

[18] Zdenek P. Bazant. *Scaling of dislocation–based strain–gradient plasticity*. Journal of the Mechanics and Physics of Solids, ISSN 0022–5096, **50**(3), 435–448 (2002). Referenciado en 102

[19] Abu Al–Rub and George Z. Voyiadjis. *Analytical and Experimental Determination of the Material Intrinsic Length Scale of Strain Gradient Plasticity Theory From Micro–And Nano–Indentation experiments*. International Journal of Plasticity, ISSN 0749–6419, **20**(6), 1139–1182 (2004). Referenciado en 102

[20] E. Cosserat and F. Cosserat. *Théorie des corps déformables*. Paris: A. Hermann & Fils, 1909. Referenciado en 104

[21] E. Aero and E. Kuvshinsky. *Fundamental equations of the Theory of elastic media with rotationally interacting particles*. Soviet Physics–Solid State, ISSN 0038–5654, **2**, 1272–1281 (1961). Referenciado en 105

[22] R. D. Mindlin. *Micro–structure in Linear Elasticity*. Archive for Rational Mechanics and Analysis, ISSN 0003–9527, **16**(1), 51–78 (1964). Referenciado en 105

[23] R. De Borst. *A generalization of J2–flow Theory for polar continua*. Computer Methods in Applied Mechanics and Engineering, ISSN 0045–7825, **103**, 347–362 (1993). Referenciado en 105

[24] R. D. Mindlin and H. F. Tiersten. *Effects of Couple-Stresses in Linear Elasticity*. Communicated by C. Truesdell, Archive for Rational Mechanics and Analysis, ISSN 0003–9527, **11**(1), 415–448 (1962). Referenciado en 105

[25] R. Toupin. *Elastic Materials with Couple–Stresses*. Archive for Rational Mechanics and Analysis, ISSN 0003–9527, **11**(1), 385–414 (1962). Referenciado en 105

[26] R. D. Mindlin. *Second gradient of strain and surface–tension in linear elasticity*. International Journal of Solids and Structures, ISSN 0020–7683, **1**(), 417–438 (1965). Referenciado en 105

[27] L. R. Herrmann. *Mixed Finite Elements for Couple–Stress Analysis* in Mixed and Hybrid Finite Element Methods. Eds. S. N. Alturi, R. H. Gallagher and O. C. Zienkiewicz. John Wiley and Sons, 1983. Referenciado en 110

[28] J. Y. Shu, W. E. King and N. Fleck. *Strain Gradient Plasticity: Size Dependent Deformation of Bicrystals*. Journal of the Mechanics and Physics of Solids, ISSN 0022–5096, **47**, 297–324 (1999). Referenciado en 110

[29] J. Y. Shu, W. E. King and N. A. Fleck. *Finite elements for materials with strain gradient effects*. International journal for numerical methods in engineering, ISSN 0029–5981, **44**(3), 373–391 (1999). Referenciado en 110

[30] Z. Xia and J. Hutchinson. *Crack Tip Fields in Strain Gradient Plasticity*. Journal of the Mechanics and Physics of Solids, ISSN 0022–5096, **44**(10), 1621–1648 (1996). Referenciado en 111

[31] Y. Wei and J. W. Hutchinson. *Steady–state crack growth and work of fracture for solids characterized by strain gradient plasticity*. Journal of the Mechanics and Physics of Solids, ISSN 0022–5096, **45**(8), 1253–1273 (1997). Referenciado en 111

[32] M. R. Begley and J. W. Hutchinson. *The mechanics of size–dependent indentation*. Journal of the Mechanics and Physics of Solids, ISSN 0022-5096, **46**(10), 2049–2068 (1998). Referenciado en 111

[33] George Z. Voyiadjis and Abu Al–Rub. *Gradient plasticity theory with variable length scale parameter*. International journal of solids and structures, ISSN 0020–7683, **42**(14), 3998–4029 (2005). Referenciado en 119

[34] Y. C. Fung and Pin Tong. *Classical and Computational Solid Mechanics* (Advanced Series in Engineering Science), ISBN 978–9810241247. World Scientific Publishing Company, 2001. Referenciado en 116